Journal of Catalysis 264 (2009) 15–30

Contents lists available at ScienceDirect

Journal of Catalysis

journal homepage: www.elsevier.com/locate/jcat

# IR spectroscopic and catalytic characterization of the acidity of imogolite-based systems

Barbara Bonelli [a,b], Ilaria Bottero [a,b], Nicola Ballarini [c,d], Sauro Passeri [c,d], Fabrizio Cavani [c,d], Edoardo Garrone [a,b,*]

[a] Dipartimento di Scienza dei Materiali e Ingegneria Chimica, Politecnico di Torino, Corso Duca degli Abruzzi 24, I-10129 Torino, Italy
[b] INSTM Unit Torino Politecnico, Italy
[c] Dipartimento di Chimica Industriale e dei Materiali, Facoltà di Chimica Industriale, Università di Bologna – Viale Risorgimento 4, I-40136 Bologna, Italy
[d] INSTM, Research Unit of Bologna, Italy

ARTICLE INFO

*Article history:*
Received 4 December 2008
Revised 19 February 2009
Accepted 8 March 2009
Available online 23 April 2009

*Keywords:*
Imogolite
Nanotubes
Alumino-silicate
FT-IR
Acidity

ABSTRACT

This paper studies the surface properties of three systems based on imogolite, as it concerns the type, acidic strength, accessibility and stability of hydroxyl groups. Proper imogolite presents a peculiar nanotube structure with remarkable surface features being the outer surface covered by Al(OH)Al groups and the inner surface lined by abundant, but presumably non-interacting, ≡SiOH groups. As a hydrated alumino-silicate, the behaviour of imogolite is very sensitive to thermal pre-treatments. Molecular water is removed only at 300 °C: this makes inner silanols accessible to probes such as CO, ammonia, methanol and, partially, to phenol. Silanols are as acidic as those of amorphous silica, but their abundance enhances the interaction with adsorbed molecules: on the one hand, ammonia is observed to form ammonium species, and on the other hand, diffusion is difficult. At temperatures around 500 °C, the nanotube structure is lost with the formation of a lamellar phase showing new stronger acidic properties, resembling those of amorphous alumino-silicates with high Al content. An amorphous precursor phase with the same chemical composition (proto-imogolite) is also available, and has been studied as were the other forms of imogolite.

Catalytic tests of gas-phase phenol reaction with methanol showed that the aromatic compound has a limited access to inner silanols at high temperature, whereas methanol interacts with both inner silanols and outer Al(OH)Al groups. Proto-imogolite shows a remarkable acid-type behaviour in phenol methylation, which, however, rapidly declines because of deactivation phenomena. A peculiar reactivity is shown by the lamellar phase: its amphoteric character, combining both basic and acidic Lewis sites, leads to a high regio-selective behaviour, and to the preferred formation of *o*-cresol.



## 1. Introduction

Proper imogolite (from the Japanese "Imogo", clay soil) is a material of volcanic origin [1] with a chemical composition $(OH)_3Al_2O_3SiOH$ and a fascinating nanotube structure [2], which is illustrated in Scheme 1. Formation of imogolite can be described considering a single $Al(OH)_3$gibbsite sheet and substituting, on one side only, three OH groups with an orthosilicate unit $O_3SiOH$. With Si–O bonds being shorter than Al–O bonds, the gibbsite-like sheet curls up, eventually forming nanotubes. When the process is not successful, an amorphous phase forms, which is proto-imogolite (Scheme 2).

Imogolite may also be obtained via sol–gel synthesis, the most common methods being those of Farmer et al. and Wada et al. [3–5], respectively. Natural imogolite nanotubes are several micrometres long, with an inner diameter and an outer diameter of 1.0 and 2.0 nm, respectively [2], whereas the outer diameter of synthetic imogolite increases to ca. 2.7 nm. Electron diffraction measurements [2] and computer models [6] showed that the most likely structures for natural and synthetic imogolite are nanotubes with 10 and 12 gibbsite units in the cross-section, respectively. These structural findings are in agreement with the recent molecular dynamics simulations, showing that the strain energy has a minimum for nanotubes with 24 Al atoms in the cross-section (corresponding to 12 gibbsite units) [7].

The structure represented in Scheme 1 for natural imogolite allows for a few considerations concerning internal silanols. The distance between two adjacent silanols in the same circumference results to be 0.26 nm and that between two silanols of two adjacent circumferences is 0.40 nm. Silanols density can therefore be

* Corresponding author. Address: Dipartimento di Scienza dei Materiali e Ingegneria Chimica, Politecnico di Torino, Corso Duca degli Abruzzi 24, I-10129 Torino, Italy. Fax: +39 0 11 564 4699.
*E-mail address:* edoardo.garrone@polito.it (E. Garrone).

0021-9517/$ - see front matter © 2009 Elsevier Inc. All rights reserved.
doi:10.1016/j.jcat.2009.03.003

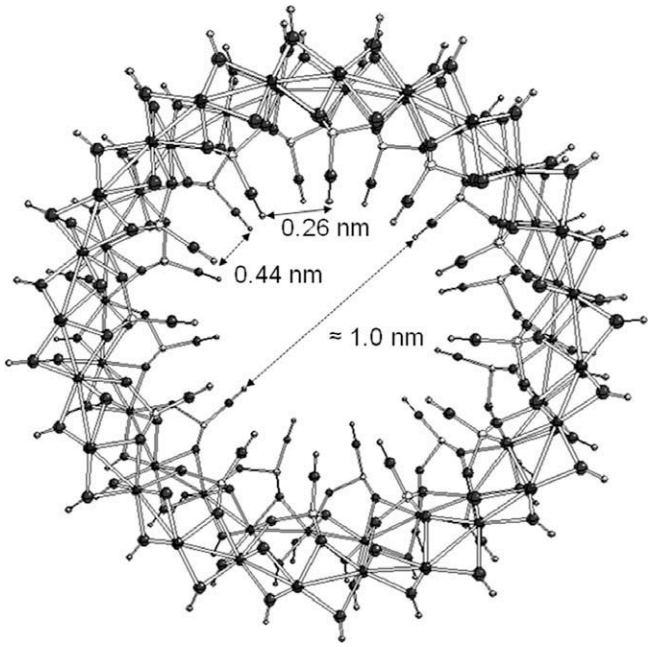


Scheme 1.

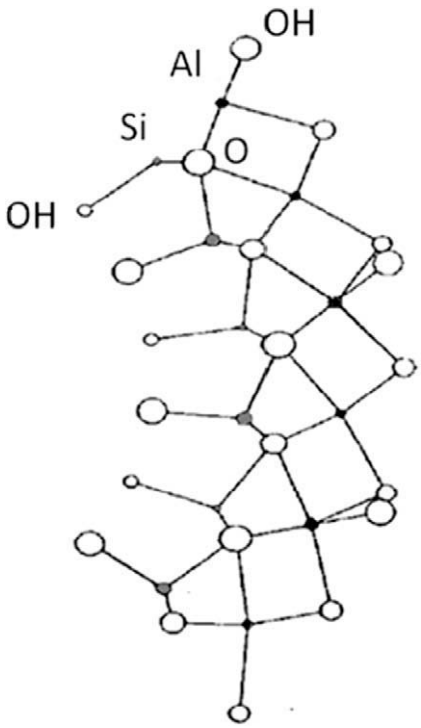


Scheme 2.

calculated through simple geometric considerations: it results to be 9.1 OH $nm^{-2}$, which is ca. twice as much as the average silanols density at the surface of hydrated amorphous silicas, which is ca. 5 OH $nm^{-2}$ [8]. Taking into account the rigidity of the pseudo-crystalline structure and the distances between them, internal silanols are expected, in spite of the remarkable surface density, not to show sizable reciprocal interactions.

Once formed, nanotubes organize into a porous network of interwoven bundles, with three kinds of pores, shown in Scheme 3: (A) intra-tube pores (about 1 nm wide); (B) inter-tube pores, the spacings between three aligned tubes in a regular packing

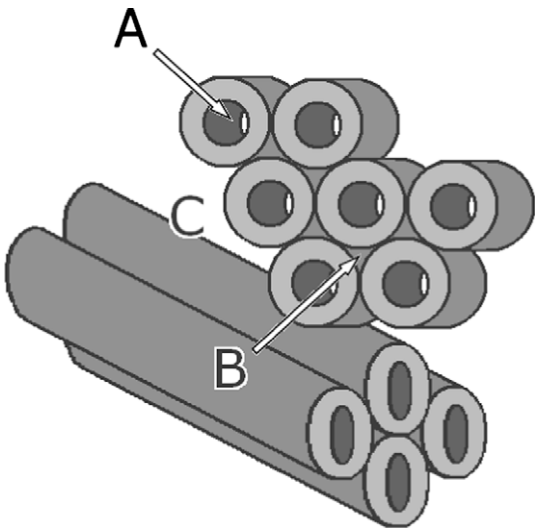


Scheme 3.

(0.3–0.4 nm wide) and (C) slit mesopores among bundles [9,10]. It is probable that inter-tube pores are too small to allow any adsorption phenomenon [9,10].

Though much less famous than carbon nanotubes, imogolite nanotubes exhibit interesting features, and offer potential applications in gas adsorption, separation and storage [6,9,10]; anions/cations retention from water [11–15] and catalysis [16,17]. The study of the surface properties, *e.g.* the type and abundance of acidic Lewis and/or Brønsted species, and of the exploitation of such systems has not been developed yet: the present paper constitutes a pioneering attempt in the field.

From a catalytic point of view, the most interesting features are (i) the nanoporous structure; (ii) the outer surface covered by Al(OH)Al groups and (iii) the inner surface lined by ≡SiOH groups. With the outer Al atoms being octahedrally coordinated, no noticeable acidity is expected for sites related to such Al species [18]. Catalytic activity, if any, should be related to inner silanols: the nanopore structure should thus be effective in promoting shape-selective diffusion of reactants by favouring the preferential formation of small products with respect to "bulky" side products.

Besides for gas–solid reactions, imogolite is also considered for aqueous phase reactions, since, depending on pH, the outer surface may carry a positive net charge [19] and the inner surface a corresponding negative net charge due to the protonation equilibria:

$$\mathrm{Al(OH)Al} + \mathrm{H^+} = \mathrm{Al(OH_2)^+Al} \quad (1)$$

$$\equiv\mathrm{SiO{-}H} = \equiv\mathrm{SiO^-} + \mathrm{H^+} \quad (2)$$

This feature probably accounts for the formation of closely packed bundles of several hundred tubes since bound counterions may hold nanotubes together [19].

Being a hydrated alumino-silicate, its hydration/dehydration behaviour is of paramount importance in dictating the operating conditions for any application requiring a surface interaction. Upon heating, imogolite starts losing physisorbed water below 200 °C, whereas loss of water because of hydroxyl condensation occurs only at about 400 °C [20], *i.e.* at a temperature higher than that required for proto-imogolite. As shown by previous studies on the structure and thermal transformation of imogolite [20], dehydroxylation at 500 °C is accompanied by the breakdown of the tubes followed by condensation and formation of a lamellar alumino-silicate with new surface functionalities (Scheme 4). Literature NMR spectra indeed show that in imogolite nanotubes only tetrahedral Si atoms and octahedral Al atoms are present. Previous studies indicate that after structural dehydroxylation new environments

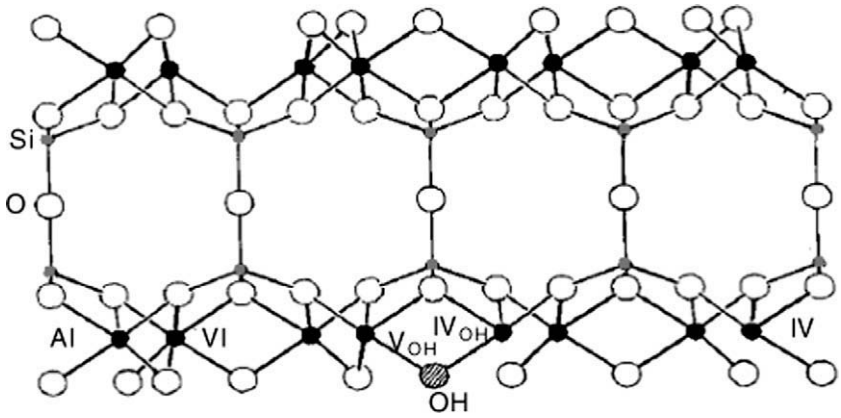


**Scheme 4.**

arise for both Si and Al [20], the latter being present also as tetrahedral and five-coordinated aluminium.

Scheme 4 shows the structure proposed in the literature for the lamellar phase, as obtained from cleavage and subsequent condensation of nanotubes: Al may be six-coordinated (site VI in the scheme), four-coordinated (site IV) and four- or five-coordinated with residual hydroxyl (sites $IV_{OH}$ and $V_{OH}$, respectively), whereas Si tends to form Si–O–Si bonds rather than silanols.

The set of three phases related to imogolite and the availability of the corresponding structural models have prompted us to investigate the surface functionalities of proper imogolite (IM), of the amorphous proto-imogolite (PR-IM) phase and of the lamellar material (L-IM) via a joint FT-IR and catalytic study. The interaction with several probe molecules (carbon monoxide, ammonia, phenol and methanol), showing quite different acid–base properties, was studied, aiming at understanding the active sites accessibility and reactivity. In this regard, the reaction between phenol and methanol was chosen as a probe test in electrophilic aromatic substitution, in particular, to check the accessibility of acidic sites in IM under flow conditions. Reactivity towards the same reaction was also measured for PR-IM and L-IM. For comparison, catalytic measurements were also carried out with alumina and silica, which are assumed to represent the reactivity of the outer and inner surfaces of IM, respectively.

Further details on the choice of this reaction are given below.

## 2. Experimental

### 2.1. Materials

Imogolite was synthesized according to Farmer et al. [3]: at 20 °C, TEOS (Tetra-ethoxysilane) and Al(s-butoxide)$_3$ were added to a 75 mM aqueous solution of $HClO_4$ in the molar ratios Si:Al:$HClO_4$ = 1,x:2:1. A slight excess of TEOS was used in order to prevent the preferential formation of aluminium hydroxide during hydrolysis. The solution was stirred for 18 h, diluted to 20 mM in Al, autoclaved at 100 °C for 4 days, dialyzed for 4 days against de-ionized water and then dried at 50 °C. Reaction conditions are rather strict, and unsuccessful syntheses lead to amorphous PR-IM.

Reference $\gamma$-$Al_2O_3$ catalyst was prepared by precipitation from an aqueous solution containing the corresponding nitrate. For instance, to obtain 10 g of $\gamma$-$Al_2O_3$, 73.56 g of $Al(NO_3)_3{}^*\ 9H_2O$ (Carlo Erba Reagenti, 99% purity) was dissolved in 196 ml of distilled water. The solution was added dropwise to another solution containing 20.78 g of $Na_2CO_3$ (Carlo Erba Reagenti) dissolved in 196 ml of distilled water. While adding the first solution to the second one, the pH was continuously adjusted to 10.0. The so-obtained slurry was left under stirring for 40 min; then the precipitate was separated from the liquid by filtration and was washed with 5 l of distilled water at 40 °C. The solid was then dried at 110 °C overnight and was calcined at 450 °C for 8 h in air. The final surface area of the calcined sample was 110 $m^2\ g^{-1}$.

Reference $SiO_2$ was Grace Silica Catalyst Support (GRACE Catalyst and Carriers) with a surface area of 291 $m^2\ g^{-1}$.

### 2.2. Methods

XRD patterns of powder samples were collected with a X'Pert Phillips diffractometer using Cu $K_\alpha$ radiation in the 2.5–20° $2\theta$ range (step width = 0.02°).

Field Emission Scanning Microscopy (FESEM) pictures were collected with a high resolution FESEM instrument (LEO 1525) equipped with a Gemini Field Emission Column.

BET surface area and pore sizes of the powders outgassed at 150 °C were measured by means of $N_2$ adsorption/desorption at −196 °C on a Quantacrome Autosorb 1C instrument. The Non-Local-Density Functional Theory (NL-DFT) method was used to evaluate pores size distribution (PSD) by applying a $N_2$–silica kernel.

NMR spectra were recorded on a Bruker Avance 400 MHz spectrometer equipped with a 9.4 T magnet operating at a frequency of 79.3 MHz for $^{29}Si$ and of 104.3 MHz for $^{27}Al$. Samples were packed in 4-mm $ZrO_2$ rotors and were rotated at MAS rates of ∼10 kHz. Spectra were recorded using recycle intervals of 1 s (Al) and 180 s (Si). 1H decoupling (∼80 kHz) was also employed, but it resulted in little difference to the linewidths observed.

IR spectra of both KBr pellets and self-supporting wafers were collected on a Equinox 55 spectrophotometer equipped with MCT cryodetector. Self-supporting wafers (with a density of about 10 mg $cm^{-2}$) were treated under high vacuum (residual pressure <$10^{-3}$ mbar) at 150, 300 and 500 °C prior to the adsorption of probe molecules. These were (a) carbon monoxide. With the interaction being very weak, FT-IR measurements were carried out at the nominal temperature of nitrogen normal boiling point (NBP); and (b) ammonia, phenol and methanol, which were adsorbed at room temperature.

In the following, samples are identified by the acronym of the solid followed by the temperature (in Celsius) of the pre-treatment, *e.g.* IM-150 stands for imogolite heated at 150 °C. Note that IM-500 coincides with L-IM: the latter acronym will be hereafter used to indicate the lamellar material.

### 2.3. Catalytic tests

Catalytic tests with PR-IM, IM-300 and L-IM were carried out by vapourization of a methanol/phenol liquid mixture (methanol/

phenol molar ratio 7/1; phenol was supplied by Sigma Aldrich, 99+% purity; methanol was supplied by Carlo Erba Reagenti) in a $N_2$ stream. The composition of the feed gas was (in molar fractions) as follows: methanol, 0.094; phenol, 0.013; and nitrogen, 0.893. Overall gas residence time was 0.78 s. Total pressure was atmospheric pressur. For catalytic tests carried out with $\gamma$-$Al_2O_3$ and $SiO_2$, the composition of the feed gas was (in molar fractions) as follows: methanol, 0.108; phenol, 0.011; and nitrogen, 0.881. The gas/vapours stream was fed to a glass reactor containing 1 $cm^3$ of catalyst shaped as 30–60 mesh particles. Catalysts weights were as follows: PR-IM, 0.92 g; IM-300 and L-IM, 0.92 g; $\gamma$-$Al_2O_3$, 0.78 g; and $SiO_2$, 0.34 g. During catalytic measurements, the reactor exit stream was condensed in 25 ml of HPLC-grade acetone for 1 h, which was maintained at 6 °C. Products condensed in acetone were analyzed by gas chromatography using a GC6000 Carlo Erba instrument equipped with a FID and a HP-5 column. The GC oven temperature was programmed from 50 to 250 °C with a heating rate of 10 °C/min.

## 3. Results and discussion

### 3.1. Textural characterization

Fig. 1 shows the low-angle XRD patterns of fresh imogolite IM, of IM-300 and of L-IM, along with that of PR-IM (inset). In agreement with the literature, PR-IM is amorphous [18], whereas IM diffraction patterns show the peaks of the hexagonal structure into which bundles of nanotubes are organized. From the (1 0 0) reflection at $2\theta = 4.18°$, a centre-to-centre distance between two adjacent nanotubes was calculated to be 2.54 nm, which is in agreement with the literature [2]. The nanotube structure is preserved at 300 °C (IM-300), notwithstanding a limited loss of long range order, whereas after treatment at 500 °C, only one peak is seen at $2\theta = 4.04°$ due to the formation of a lamellar phase [19].

Fig. 2a shows $N_2$ isotherms at −196 °C: with PR-IM, IM-150 and IM-300, Type I isotherms are observed, typical of microporous materials, with small hysteresis loops due to limited external mesoporosity, most probably deriving from slit mesopores among bundles (Scheme 3).

With L-IM, a more pronounced hysteresis loop is observed, accompanied by a loss of specific surface area (SSA), due to structure collapse. As reported in Table 1, PR-IM has the lowest BET SSA (178 $m^2\,g^{-1}$), which then increases when passing from IM-150 (213 $m^2\,g^{-1}$) to IM-300 (362 $m^2\,g^{-1}$). The smaller BET SSA of IM-150 with respect to IM-300 indicates that the pores of the former sample are still partially filled with water and therefore are not accessible to $N_2$. This conclusion is confirmed by the corresponding Pores Size Distributions (Fig. 2b) determined from the adsorption branches of isotherms shown in Fig. 2a: with IM-300, a definite peak is observed corresponding to micropores with 0.98 nm diameter, in fair agreement with structural data. IM-150, instead, only shows heterogeneous pores with a diameter >1.5 nm: the treatment at 300 °C allows access to imogolite nanovoids, still preserving the nanotube structure, probably as a consequence of water removal from micropores with 0.98 nm diameter. This conclusion is supported by the fact that both total and microporous volumes increase from IM-150 to IM-300 (Table 1).

Larger pores are instead due to heterogeneous inter-bundles voids in the fibrous network shown by the FESEM picture in Fig. 3. PR-IM appears instead as hollow spheres, as reported in the inset at a lower magnification.

Fig. 4a shows the $^{29}$Si-MAS NMR spectrum of fresh IM, which shows an intense resonance peak at $\delta = -79$ ppm: this highly shielded shift is characteristic of the imogolite structure and is assigned to isolated Si tetrahedron centres ($Q_0$ sites) sharing three oxygen atoms with octahedral Al atoms [20,21]. The spectrum also shows a minor shoulder at $\delta = -86$ ppm, probably due to the limited occurrence of an amorphous phase, since it was previously observed in unheated natural allophane and synthetic aluminosilicate gels [20,21].

The $^{27}$Al NMR spectrum of fresh IM (Fig. 4b) presents a main peak at $\delta = 5.5$ ppm close to that of gibbsite ($\delta = 7.8$ ppm), indicating the presence of octahedral aluminium atoms [22]. This spectrum also exhibits a very small peak at about 60 ppm (inset), which is due to a minor amount of four-coordinated aluminium atoms, along with a small contribution from the second spinning-sideband of the major peak. In agreement with the literature [20,21], the $^{27}$Al NMR spectrum of fresh IM predominantly indicated octahedral Al, and the small amount of tetrahedral Al [21] most probably belongs to an amorphous phase rather than to nanotubes.

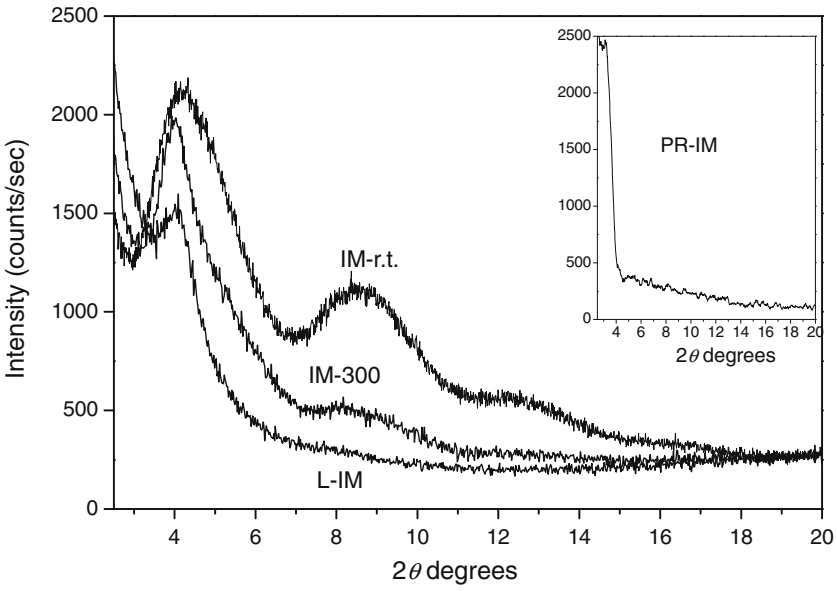


**Fig. 1.** Low-angle ($2\theta = 2.5$–$20°$) powder XRD patterns of fresh imogolite (IM-r.t.), IM-300 and L-IM. Inset to the figure: powder XRD patterns of proto-imogolite (PR-IM).

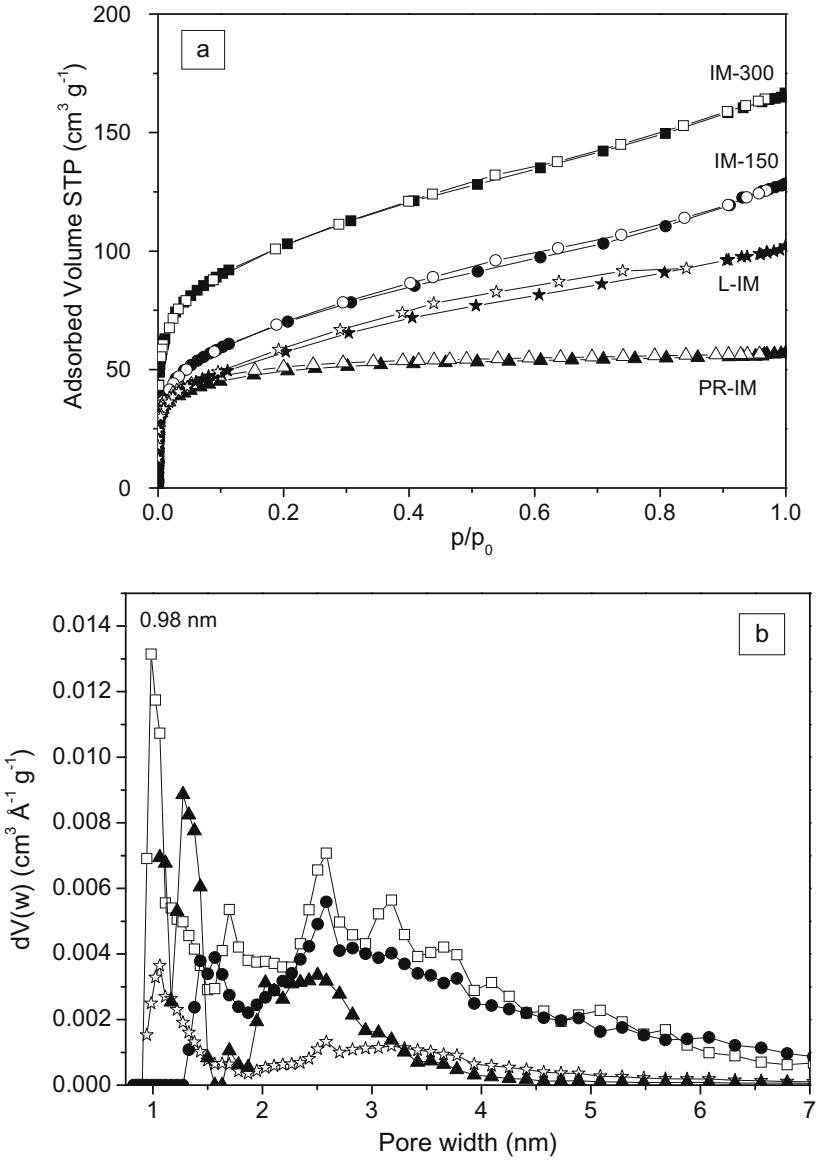


**Fig. 2.** (a) $N_2$ adsorption/desorption isotherms at −196 °C on PR-IM (triangles); IM-150 (circles); IM-300 (squares) and L-IM (stars). Full symbols: adsorption branch; white symbols: desorption branch. (b) NL-DFT Pore Size Distributions (PSD) obtained from absorption branches of the corresponding isotherms: IM-150 (full circles); IM-300 (white squares); L-IM (white stars) and PR-IM (full triangles).

**Table 1**
Textural features of imogolite and proto-imogolite as derived from combined XRD patterns and $N_2$ isotherms at −196 °C.

| Sample | BET SSA ($m^2\ g^{-1}$) | Total pore vol. ($cm^3\ g^{-1}$) | Micropores vol. ($cm^3\ g^{-1}$)[a] | Inner diameter (nm)[b] | Outer diameter (nm)[c] |
|---|---|---|---|---|---|
| IM-150 | 213 | 0.20 | 0.01 | – | – |
| IM-300 | 362 | 0.26 | 0.04 | 0.98 | 2.44 |
| L-IM | 197 | 0.16 | 0.02 | – | – |
| PR-IM | 178 | 0.09 | 0.03 | – | – |

[a] As evaluated by applying the α-s method.
[b] As evaluated by applying the NL-DFT method to the adsorption branch of the isotherm.
[c] As evaluated by the $d_{(100)}$ reflection of the XRD spectrum.

### 3.2. FT-IR spectroscopic characterization of bare samples

Fig. 5 shows the IR spectra of an IM self-supporting wafer outgassed at r.t., 150 and 300 °C, and of L-IM. In the hydroxyls stretch region (3800–3000 $cm^{-1}$), spectra are dominated by intense structure-less absorption due to H-bonded species. Besides adsorbed molecular water, IM nanotubes present surface hydroxyls, both external and internal: the former may interact, besides with water molecules, also with neighbouring nanotubes. As a whole, individual contributions cannot be singled out, nor it is even possible to discriminate between inner silanols and outer aluminols. At lower wave numbers, bands at 1595 and 1465 $cm^{-1}$ are seen, assigned to carbonate-like species on the outer surface, like those formed on aluminium hydroxide [18]. The dotted vertical line at 1650 $cm^{-1}$

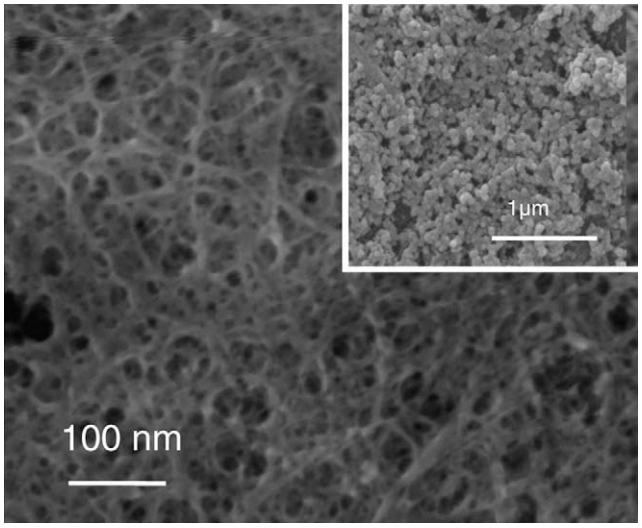


**Fig. 3.** FESEM (Field Emission Scanning Electron Microscopy) picture of fresh IM. Inset to the figure: SEM picture of PR-IM taken at lower magnification.

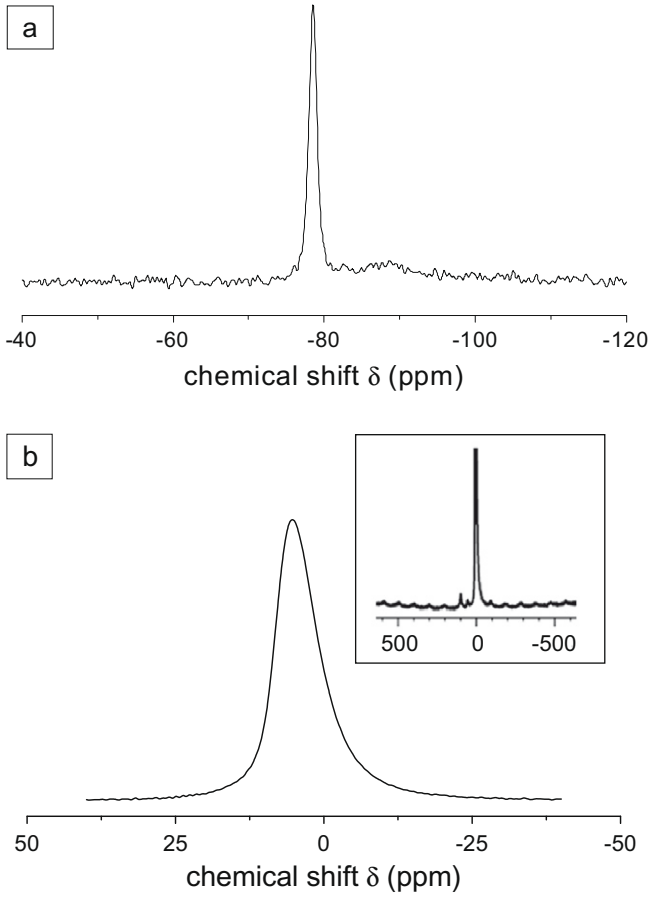


**Fig. 4.** Solid-state $^{29}$Si-MAS NMR (section a) and $^{27}$Al-MAS NMR (section b) spectra of fresh IM.

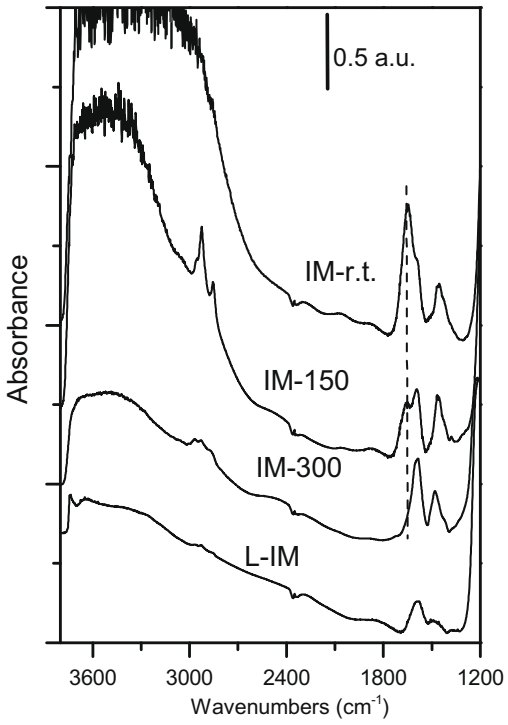


**Fig. 5.** IR spectra of imogolite outgassed for 1 h at r.t. (IM-r.t.); 150 °C (IM-150); 300 °C (IM-300) and 500 °C (L-IM).

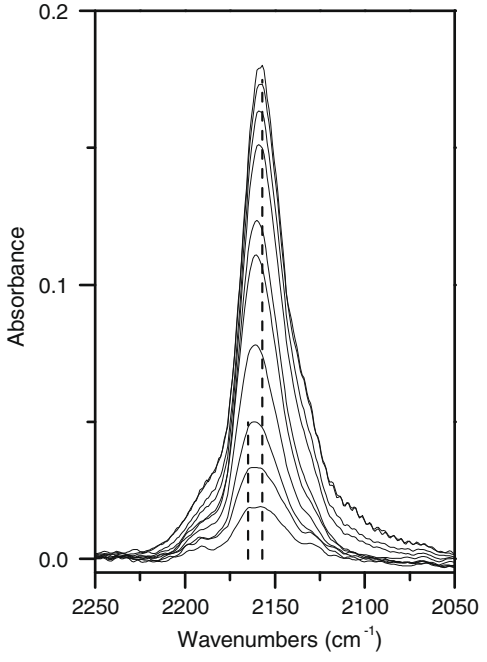


**Fig. 6.** CO stretch range (2250–2050 cm$^{-1}$) of difference IR spectra obtained after dosing CO (equilibrium pressures: 0.5–15 mbar) on PR-IM outgassed at 300 °C.

indicates the band due to the bending mode of water, removed at 300 °C. At this temperature, nanotubes are still stable (Fig. 1) and inner pores with 0.98 nm diameter become accessible (Fig. 2b).

It may be concluded that water present at both the external and internal surfaces is removed at 300 °C, rendering inner ≡SiOH groups accessible to probes.

With L-IM, the hydroxyl spectrum dramatically changes: several components are seen at 3743, 3734 and 3646 cm$^{-1}$, with a broad signal at lower frequencies due to H-bonded hydroxyls. The reference structure is the literature model represented in Scheme 4 describing a new lamellar alumino-silicate with high Al content (Al/Si = 2). However, the richness and complexity of hydroxyl species observed in Fig. 5 seem to indicate that other

processes are taking place may be with segregation of an alumina-like phase and formation of new OH species.

### 3.3. FT-IR spectroscopic characterization of acidic species: adsorption of CO and $NH_3$

To study both accessibility and acidity of OH species, CO has been dosed on all the materials at the nominal NBP of $N_2$: in the presence of free-silanols, a band at 2156 $cm^{-1}$ is expected, which is characteristic of the stretching mode of CO interacting with ≡SiOH [23].

Fig. 6 shows the spectra in the 2250–2050 $cm^{-1}$ range recorded after CO dosage on PR-IM outgassed at 300 °C: at low CO pressures, the main band shows two components (dotted lines) at 2166 and 2157 $cm^{-1}$, the latter becoming prominent at higher pressures. As reported previously, proto-imogolite is the result of failed synthesis and forms when nanotubes do not close up (Scheme 2): the two components observed in the IR spectra at 2157 and 2166 $cm^{-1}$ are assigned to CO adsorbed on silanols and on more acidic hydroxyls, respectively, as depicted in the scheme. The poor transparency of the sample in the OH stretch region did not allow to obtain reliable IR spectra in that region. However, according to the linear correlation reported in the literature [24] between the shift of perturbed hydroxyls, $\Delta\nu$(OH), and the $\nu$CO of carbon monoxide adsorbed onto OH at the surface of several zeolites and silico-aluminas, a band at 2166 $cm^{-1}$ should correspond to hydroxyls undergoing a shift $\Delta\nu$(OH) of ca. 200 $cm^{-1}$, *i.e.* OH species on the one hand being more acidic than silanols, and on the other hand, being less acidic than bridged OH groups in zeolites. The weak band at 2190 $cm^{-1}$ is assigned to CO adsorbed on the small amount of weak $Al^{3+}$ Lewis acidic sites [25].

Fig. 7 compares the relevant spectra in the 2250–2050 $cm^{-1}$ range obtained with IM-150 and IM-300 after subtraction of bare samples spectra shown in Fig. 5.

With IM-150 (lower part of Fig. 7), only one band is observed at 2148 $cm^{-1}$: the limited shift with respect to the free molecule in gas phase (2143 $cm^{-1}$) indicates a weak interaction of electrostatic nature. The observed wave number (2148 $cm^{-1}$) is close to that reported in the literature for $CO/H_2O$ dimeric complexes (2144–2149 $cm^{-1}$) formed after CO adsorption on ice: this suggests a weak interaction of CO with water molecules, probably at the outer surface [26].

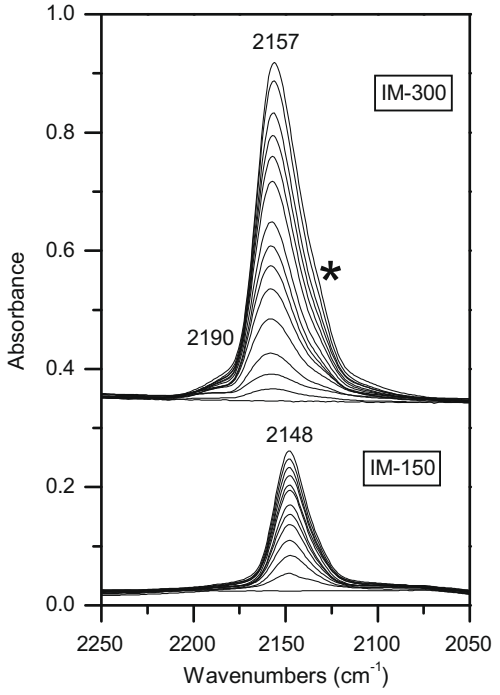


**Fig. 7.** CO stretch range (2250–2050 $cm^{-1}$) of difference IR spectra, obtained after dosing CO (equilibrium pressures: 0.5–15 mbar) on IM-150 (lower part of the figure) and IM-300 (upper part of the figure).

With IM-300 (upper part of Fig. 6), the expected band at 2157 $cm^{-1}$ due to CO on inner silanols is observed [23] together with a minor band at ca. 2190 $cm^{-1}$ probably due to CO adsorbed on weak $Al^{3+}$ Lewis sites at the outer surface [25]. Finally, the shoulder at 2131 $cm^{-1}$ (asterisk), more clearly seen at higher equilibrium pressures, is ascribed to SiOH···OC complexes previously observed on silica [27].

Fig. 8 shows the difference spectra recorded under comparable CO pressures on L-IM: as a whole, bands are less intense, indicating that fewer sites are accessible to this probe. In the CO stretching range (Fig. 8a), a weak band is seen at 2203 $cm^{-1}$, shifting with coverage to 2188 $cm^{-1}$, together with a main band at 2170 $cm^{-1}$, shifting to 2166 $cm^{-1}$. Both bands are reversible upon evacuation at low temperature: the former is assigned to CO adsorbed onto coordinatively unsaturated $Al^{3+}$, like those at the surface of transition aluminas [18], the latter to CO interacting with hydroxyls more acidic than silanols: interestingly, no band was observed at 2157 $cm^{-1}$, corresponding to CO adsorbed on accessible silanols, in fair agreement with the model shown in Scheme 4 [20].

Fig. 8b shows the OH stretch region (3800–3000 $cm^{-1}$) of the spectra represented as bold curves in Fig. 8a. Difference spectra are reported, so that negative bands correspond to hydroxyls interacting with CO and broad positive absorption corresponds to H-bond formation. Note that the sharp positive peak at 3750 $cm^{-1}$ is due to changes in the temperature of the sample as a function of the CO pressures, affecting the location of the SiO–H stretch, often observed during the experiments run at the NLP of $N_2$.

The negative band of hydroxyls interacting with CO is rather broad, indicating heterogeneity of sites: at least three components may be figured out at 3743, 3725 and 3660 $cm^{-1}$ that are shifted downward by 233, 245 and 210 $cm^{-1}$, respectively, in agreement with the literature [24] reporting a $\Delta\nu$(OH) of 200–240 $cm^{-1}$ for a $\nu$CO of 2166–2170 $cm^{-1}$.

The observed shifts are too large to be due to SiOH or AlOH species since silanols suffer with CO a shift of about 100 $cm^{-1}$ [23], whereas hydroxyls at the surface of transition aluminas suffer a hypsochromic shift by 70–95 $cm^{-1}$ [18,24], and have to be ascribed to more acidic Brønsted-like sites.

In order to understand their nature, reference may be made to previous work on zeolites or amorphous alumino-silicates. With various zeolites suffering dealumination, a band at 3670 $cm^{-1}$ was sometimes assigned to hydroxyls less acidic than proper Brønsted zeolitic sites (undergoing a downward shift by about 200 $cm^{-1}$), still partially anchored to the zeolite framework [24,28–32]; in Al-rich micelle-templated silicates with composition similar to that of L-IM (Al/Si = 0.4), hydroxyls at 3660 $cm^{-1}$ shifting with CO by ca. 220 $cm^{-1}$ were ascribed to buried Si–O–Al(OH)–O–Si species [25]; on amorphous alumino-silicates with Al/Si in the 1.0–2.0 range, hydroxyls absorbing at 3748 $cm^{-1}$ were observed to shift by ca. 230 $cm^{-1}$, the corresponding CO stretch mode being at 2169 $cm^{-1}$ [33].

The model of dehydroxylated imogolite proposed by MacKenzie [20], shown in Scheme 4, shows that the lamellar structure has basically five-coordinated Al, together with a few four- and six-coordinated sites and some residual hydroxyl groups, which should be responsible for the acidic behaviour of this material and for bands observed in the OH stretch range.

Two hypotheses can be advanced, none fully convincing. On the one hand, we may accept Scheme 4 as really depicting the system. Because in the present case the parent material (IM) is not a zeolite

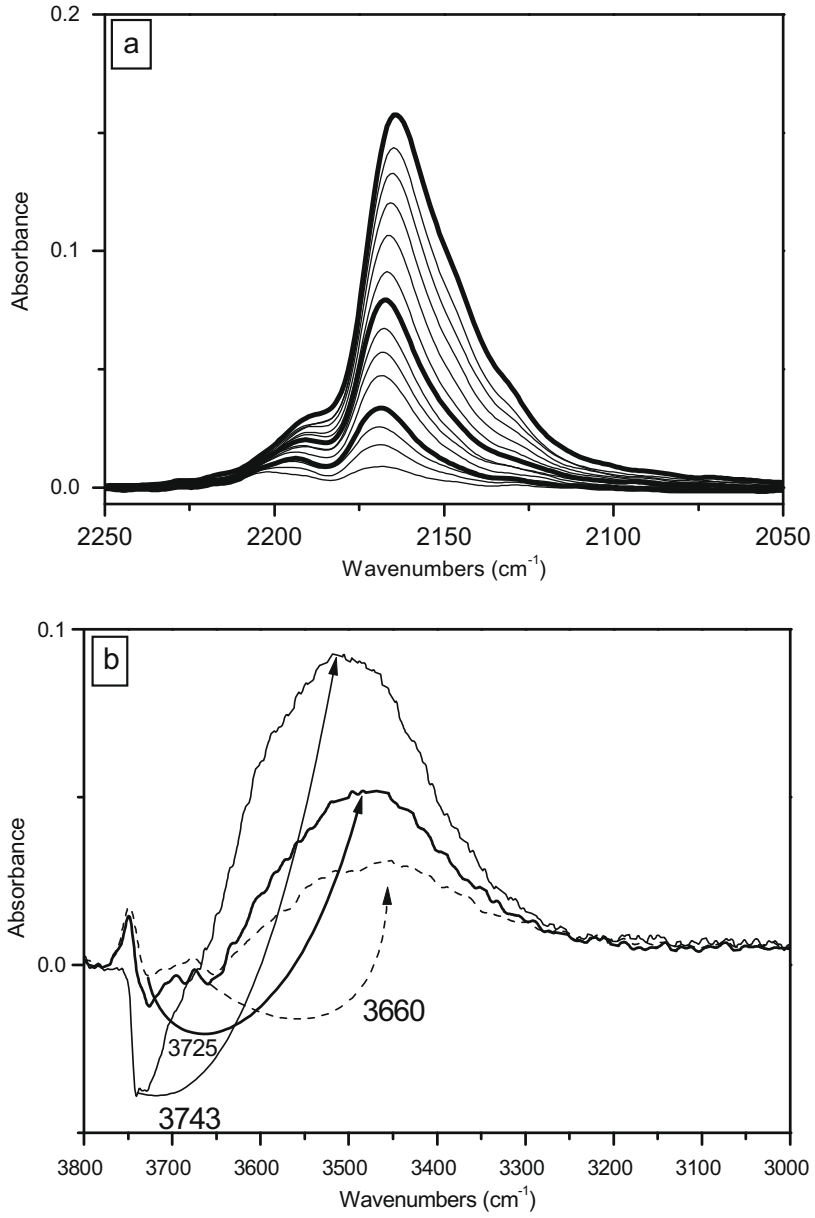


**Fig. 8.** (a) CO stretch range (2250–2050 $cm^{-1}$) of difference IR spectra obtained after dosing CO on L-IM (equilibrium pressures: 0.5–15 mbar). (b) OH stretch region (3800–3000 $cm^{-1}$) of bold curves shown in Fig. 6a.

and should probably not follow the Loewenstein rule, the high Al content could allow the formation of new OH bridged between two Al atoms, as those shown in Scheme 4. On the other hand, if Scheme 4 is accepted as only partially describing the actual system, one could imagine that the large Al content might lead to a process similar to dealumination with structural consequences that are not readily describable.

Although the issue of the acidity of L-IM cannot be satisfactorily understood, as a whole, a set of Brønsted sites of increased acidity is formed with respect to those present at the surface of IM, a feature that renders L-IM probably interesting as an acidic catalyst.

After ammonia dosage on PR-IM outgassed at 300 °C (sample PR-IM-300, Fig. 9a), bands are seen at 1625, 1450 and 1300 $cm^{-1}$: the two bands at 1625 and 1300 $cm^{-1}$ are, respectively, ascribed to the anti-symmetric and symmetric bending modes of ammonia sitting on $Al^{3+}$ Lewis sites [34], whereas that at 1450 $cm^{-1}$ is due to ammonium species formed on Brønsted acidic sites, such as those occurring upon ammonia adsorption on Brønsted sites inside zeolites microcavities [35]. Interaction with ammonia is only reversible at 300 °C, indicating the presence of medium-strength acidic sites. Besides, at higher equilibrium pressures, ammonia also interacts via H-bonding with silanols, giving rise to the broad band at ca. 3000 $cm^{-1}$. The hydroxyls involved in $NH_4^+$ formation are those visible as a negative broad band in the region 3770–3630 $cm^{-1}$.

Upon $NH_3$ dosage on IM-150, bands are seen at 1625, 1450 and 1300 $cm^{-1}$ (Fig. 9b). The 1625 and 1300 $cm^{-1}$ bands are due to $NH_3$ molecules coordinated to outer $Al^{3+}$ Lewis sites; the 1450 $cm^{-1}$ band is due to $NH_4^+$ species. Correspondingly, in the OH stretch region, a sharp band decreases at 3750 $cm^{-1}$, and a broad absorption increases at about 2935 $cm^{-1}$. The limited width of the 3750 $cm^{-1}$ is probably evidence that silanols are not interacting with one another, even on the densely populated inner surface. At higher coverage, the mode of H-bonded hydroxyls is at a lower frequency than those shown in Fig. 9a and Fig. 9c. This is probably evidence that ammonia interacts, besides the silanols, with water molecules

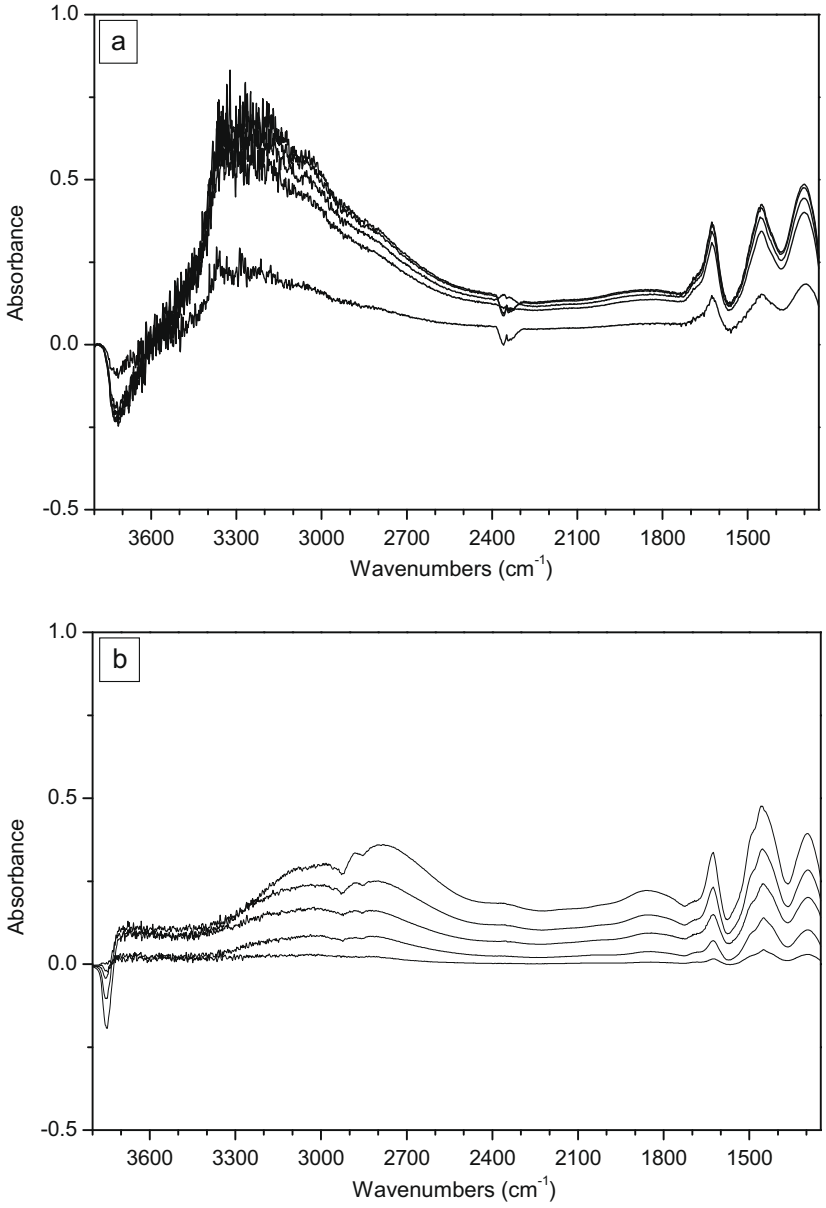


**Fig. 9.** Difference IR spectra obtained after dosing increasing $NH_3$ on PR-IM-300 (a); IM-150 (b); IM-300 (c) and L-IM (d) (equilibrium pressures: 0.5–25 mbar).

still present in the IM-150 sample, and not on the more dehydrated PR-IM-300 and IM-300. Similar considerations apply to the ammonium species (band at 1450 $cm^{-1}$).

Besides these features, spectra are complicated by the Fermi resonance (Evans window at about 2930 $cm^{-1}$) with the overtone of the $NH_4^+$ mode at 1450 $cm^{-1}$ and combination bands at about 2380 and 1850 $cm^{-1}$ [35].

Interaction with ammonia is only reversible after outgassing at 500 °C, *i.e.* at a higher temperature than that required for protoimogolite: this is probably ascribable to difficult diffusion of ammonia inside the nanotubes, still partially filled with water.

Similar spectral features are observed after $NH_3$ dosage on IM-300 (Fig. 9c). The negative band of silanols interacting with ammonia is broader probably because after water removal at 300 °C all silanols are accessible to $NH_3$ and some heterogeneity may arise, *e.g.* between those inside the nanotubes and silanols at the opening.

With L-IM (Fig. 9d), adsorption of $NH_3$ reveals the presence of both Lewis and Brønsted sites, and a component at 3660 $cm^{-1}$ (asterisk) is clearly seen, in agreement with CO adsorption, confirming the presence of more acidic OH species.

### *3.4. FT-IR characterization of hydroxyls accessibility to reactants of catalytic tests: adsorption of phenol and methanol at room temperature*

Further FT-IR measurements were performed basically on IM-300, the sample showing both accessible silanols and nanotube structure.

Fig. 10a shows the difference spectra obtained by increasing methanol equilibrium pressure (0.05–5 mbar): 2963 and 2844 $cm^{-1}$ bands are due to the $\nu_s(CH_3)$ and $2\delta_s(CH_3)$ modes, respectively: in the lower wave numbers range, the $\delta(CH_3)$ bending modes are seen. The negative band in the OH stretch range is due to silanols interacting with the OH group of methanol. As with ammonia, interaction with methanol is reversible above 300 °C.

Fig. 10b shows the difference spectra collected after dosing 0.05–2.5 mbar of phenol: in the OH stretch range

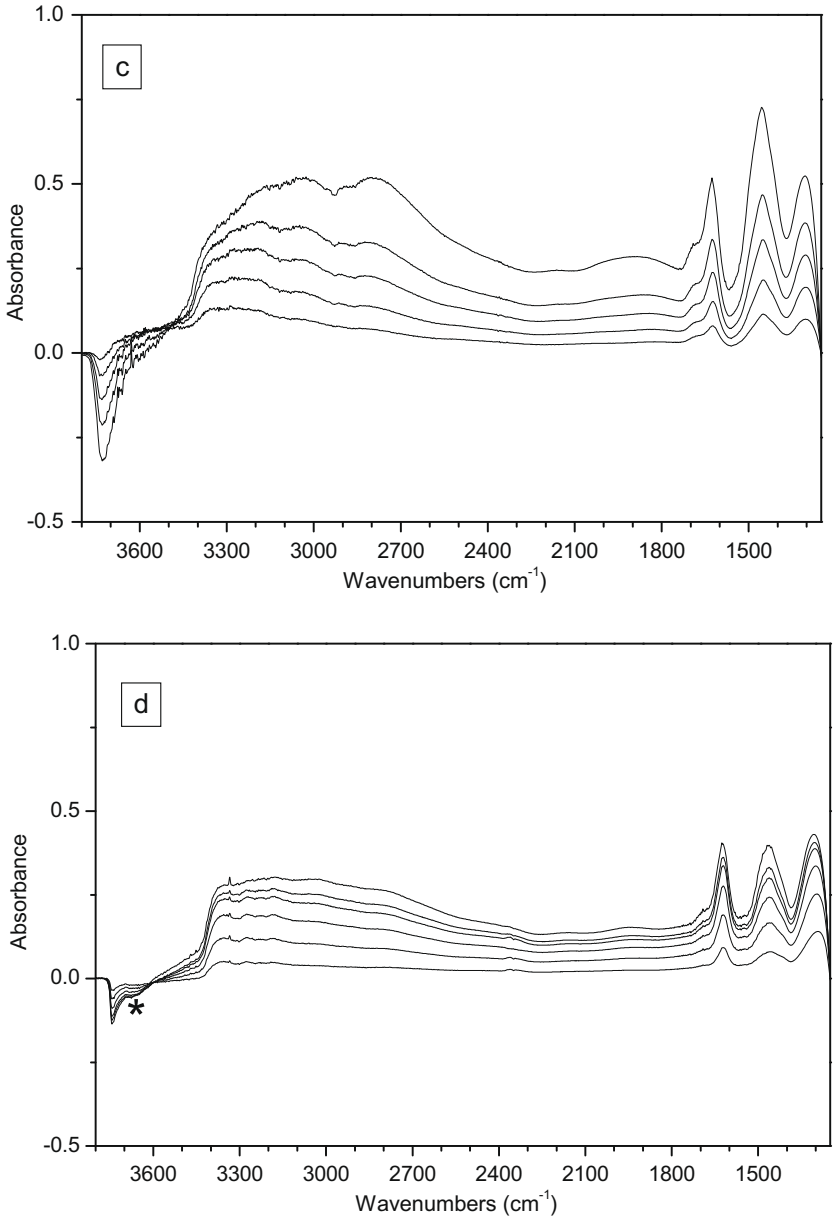


**Fig. 9** (*continued*).

(3800–2800 $cm^{-1}$), the negative band of hydroxyls interacting with phenol is very weak, indicating that few silanols are accessible to this probe in the adopted experimental conditions, *i.e.* at room temperature in static operation. It must be noted that the minimum Van de Waals diameter of phenol is 0.57 nm, *i.e.* about one-half of nanotubes inner diameter. Due to H-bond with phenol, the silanols stretching mode is shifted by ca. −400 $cm^{-1}$, as observed when dosing phenol on an amorphous silica used for comparison (spectra not shown).

Interaction with phenol is reversed after outgassing for 1 h at 300 °C, indicating a strong interaction, most probably with adsorbing sites at the outer surface.

In order to understand the nature of adsorbed phenol, Fig. 10c compares the spectra of phenol in the C═C ring stretch range adsorbed on a KBr disk (curve 1), amorphous silica (curve 2), IM-300 (curve 3), PR-IM-300 (curve 4) and L-IM (curve 5).

Phenol adsorbed on silica (curve 2) shows (i) a band at 1598 $cm^{-1}$ with a shoulder at 1605 $cm^{-1}$, assigned to the modes 8b and 8a of the aromatic ring; (ii) two bands at 1499 and 1472 $cm^{-1}$ due to the modes 19a and 19b and (iii) a broad envelop of bands below 1400 $cm^{-1}$, assigned to the in plane C–O–H bending vibration [36].

Interestingly, after adsorption of phenol on IM-300 (curve 3), a new component is seen at 1492 $cm^{-1}$, and the in plane C–O–H bending vibration bands become less intense. This may indicate that phenol is interacting not only with inner silanols, but also with other species located at the outer surface of nanotubes.

With L-IM (curve 5), the component at 1605 $cm^{-1}$ and the C–O–H bending vibration are absent, and the band at 1492 $cm^{-1}$ is as intense as that at 1499 $cm^{-1}$. These features, previously observed after phenol adsorption on alumina and Na–X zeolite, were ascribed to phenol de-protonation with the formation of surface phenolate species [36,37]. This is evidence that L-IM has a basic-type behaviour since it strips the phenolic proton of the –OH group. The broad band seen with IM-300 and L-IM around 1640 $cm^{-1}$

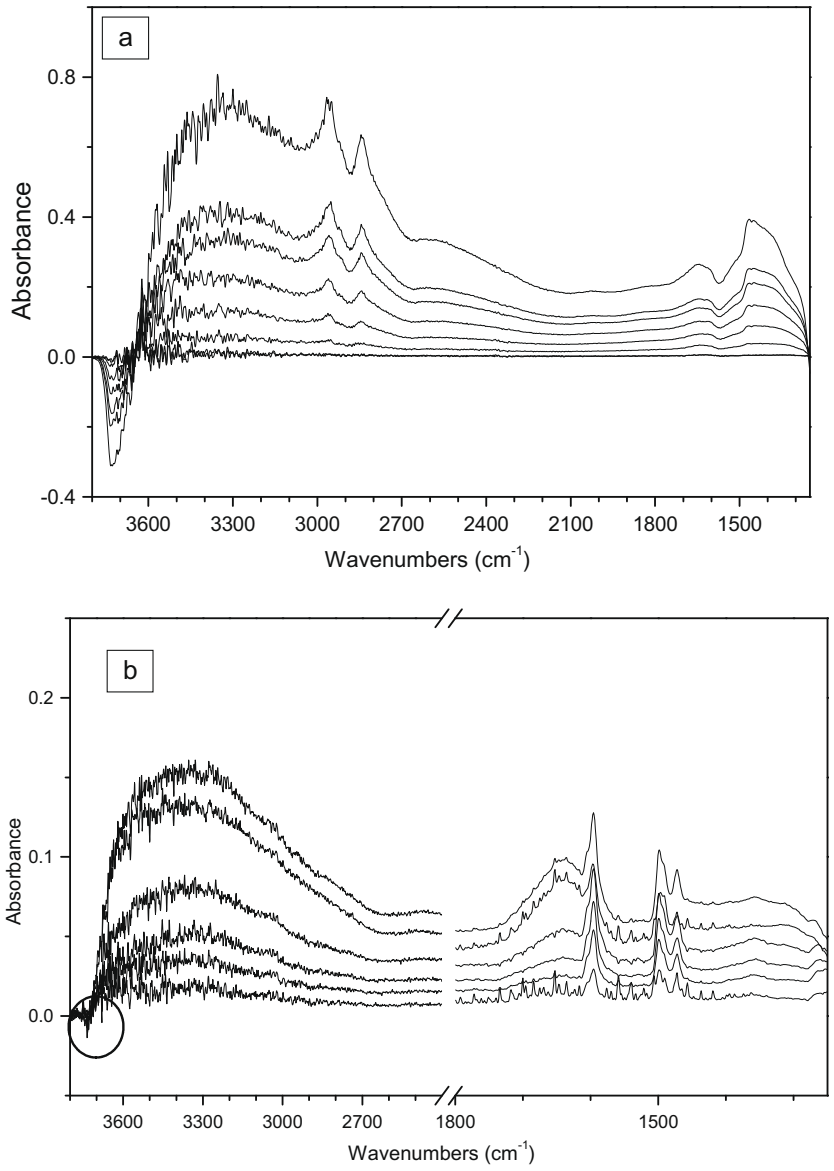


**Fig. 10.** Difference IR spectra recorded on IM-300 after dosing (a) phenol (equilibrium pressures: 0.05–2.5 mbar) and (b) methanol (equilibrium pressures: 0.05–5.0 mbar). (c) C=C aromatic ring stretch range of spectra of phenol in KBr disk (1) and adsorbed on silica (2); IM-300 (3); PR-IM-300 (4) and L-IM (5).

can be due to the formation of water by the reaction of basic surface hydroxyls with phenolic proton.

The shoulder observed at 1492 $cm^{-1}$ after adsorption of phenol on silica (curve 2) most probably has a different origin, as it could be due to the reaction of phenol with some strained (more reactive) Si–O–Si bridges, usually present at the surface of dehydrated silicas [38], with the formation of Si–O–$C_5H_6$ and SiOH species.

As to silanols acidity and accessibility, results reported in this work show that silanols behave as free silanols, in that the observed shift with ammonia, methanol and phenol is the same as on silica and the CO stretch band is at 2157 $cm^{-1}$, but their abundance at the inner surface of nanotubes enhances the strength of interaction between the surface and the adsorbed molecules, thus hindering their diffusion inside nanotubes.

Multiple interactions of silanols with molecules such as water, ammonia, methanol and phenol could explain unexpected phenomena such as (i) the high temperature of water removal (300 °C) and (ii) the formation of irreversible ammonium species by interaction of ammonia with relatively weak Brønsted acids as silanols.

At the same time, in contrast to the high pliability of Si–O–Si bonds in amorphous silicas [8], the structural stiffness of imogolite nanotubes does not allow silanols condensation without structural collapse, so rendering imogolite more similar to crystalline silica-based materials, *e.g.* silicalite.

### *3.5. Catalytic results of gas-phase phenol methylation with methanol*

This reaction was chosen as a test reaction because of the following reasons:

1. Adsorption tests showed that both molecules, phenol and methanol, may interact with the silanols in imogolite. The acidity of these sites, although very weak, is strong enough to activate these molecules. However, indications were derived that the access of molecules to these moieties might be hindered. The two reactants possess very different molecular size, and are supposed to have quite different diffusivity properties. Therefore, they can be used to discriminate the access to external Al(OH)Al and internal Si–OH sites in imogolite.

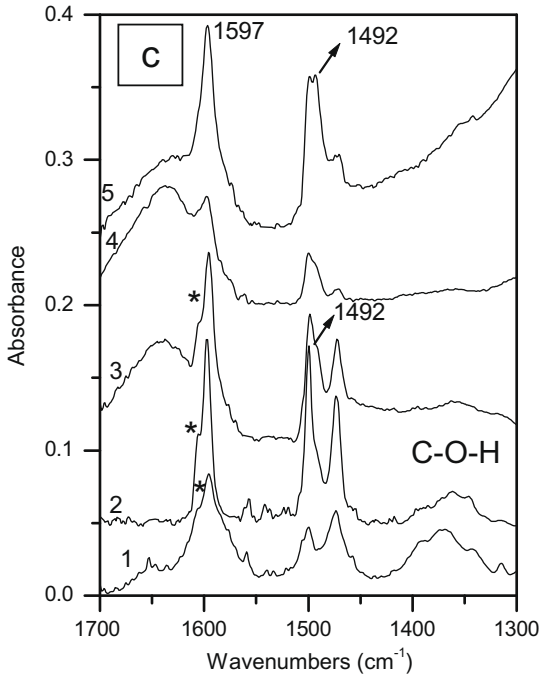


**Fig. 10** (*continued*).

2. The gas-phase alkylation of phenol is a facile reaction that may occur on either acidic or basic sites, even with sites having weak strength [39,40]. Moreover, the nature of the products formed is affected by the strength of the active sites; in general, weaker sites lead to the preferred formation of O-alkylation products (anisole), whereas stronger sites lead preferentially to C-alkylation with the production of cresols and polyalkylated phenols. Therefore, this reaction can be used as a tool for the characterization of active sites reactivity.
3. Methanol itself may undergo side reactions with formation of dimethylether first, and then of aliphatic and aromatic hydrocarbons, which are precursors of coke [41]. The latter reactions are catalyzed by strong acidic sites, and therefore they should not occur with weak acidic sites. Therefore, transformations occurring on methanol may also provide information on the active site accessibility under gas-flowing conditions.

### 3.5.1. The reactivity of PR-IM

Fig. 11 shows the effect of the reaction temperature on the catalytic performance of PR-IM. The material showed a relevant catalytic activity, giving 27% phenol conversion at 300 °C. At this temperature, the main products were *o*-cresol, polyalkylated phenols and anisole; *p*-cresol and polyalkylated anisoles formed in lower amount.

The distribution of products at 300 °C was similar to that typically observed with H-mordenites and H-β zeolites [42]. However, when the reaction temperature was increased, deactivation took place with a remarkable decline of phenol conversion. At the same time, the selectivity to polyalkylated phenols decreased, and that to *o*- and *p*-cresol increased due to the decreased contribution of consecutive reactions. The deactivation behaviour was also quite similar to that observed for zeolites due to the accumulation of coke formed by the hardening of aliphatic and aromatic hydrocarbons originated by methanol transformation [43,44].

The deactivation of PR-IM was confirmed by measurements made on the fresh catalyst, which was recorded as a function of the reaction time (Fig. 12). The progressive decrease of phenol conversion led to an increase of selectivity to *o*-cresol and to a decrease of that to polyalkylated phenols. Surprisingly, the selectivity to anisole was not affected by the change of phenol conversion, and that to *p*-cresol decreased and became nil after 2 h reaction time. This means that the formation of polyalkylated aromatics occurred by transformation of *o*-cresol, whereas the para isomer did not undergo consecutive reactions. The spent catalyst was fully coked, confirming the acidic properties of this material.

These tests demonstrate that the amorphous material, precursor of imogolite formation, has medium-strength acid sites that are fully accessible to both phenol and methanol, in agreement with characterization tests done by adsorption of probe molecules.

### 3.5.2. The reactivity of IM-300 and L-IM

Reactivity tests were carried out with the imogolite after thermal treatment at 300 °C (IM-300) and at 500 °C (L-IM, Fig. 13).

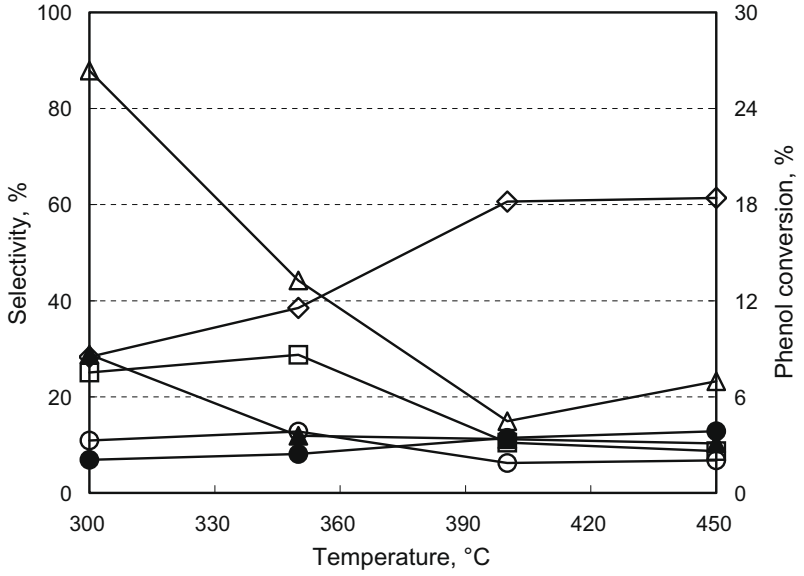


**Fig. 11.** Effect of temperature on catalytic performance of PR-IM. Symbols: phenol conversion (△), selectivity to *o*-cresol (◇), selectivity to anisole (▲), selectivity to *p*-cresol (●), selectivity to 2,6-xylenol (○) and selectivity to other polyalkylated aromatics (□).

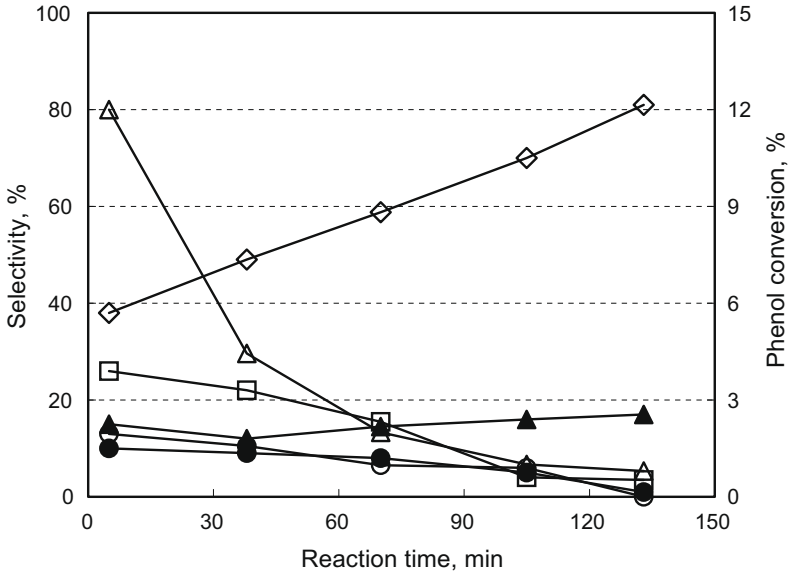


**Fig. 12.** Effect of reaction time on catalytic performance of PR-IM. Symbols: phenol conversion (△), selectivity to *o*-cresol (◇), selectivity to anisole (▲), selectivity to *p*-cresol (●), selectivity to 2,6-xylenol (○) and selectivity to other polyalkylated aromatics (□). Temperature 350 °C.

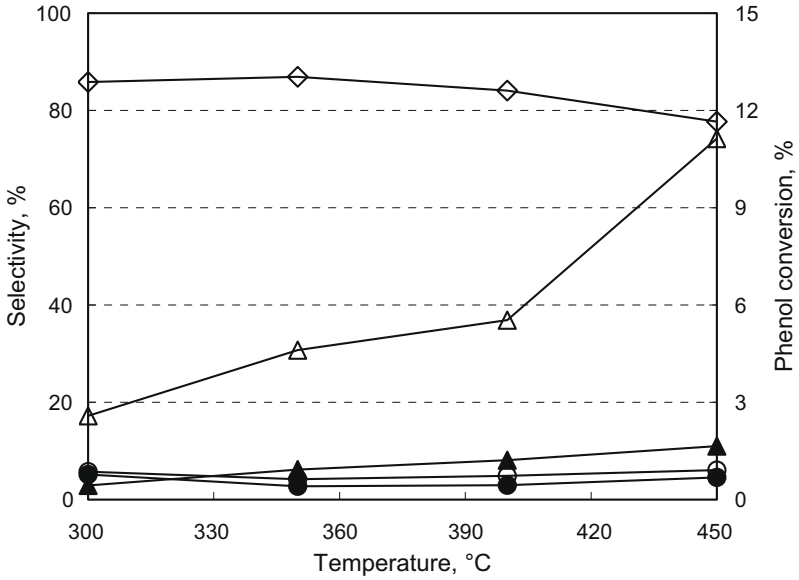


**Fig. 13.** Effect of temperature on catalytic performance of L-IM. Symbols: phenol conversion (△), selectivity to *o*-cresol (◇), selectivity to anisole (▲), selectivity to *p*-cresol (●) and selectivity to 2,6-xylenol (○).

Sample IM-300 was inactive at 300 °C; in fact, the phenol conversion was 0.03%, which was remarkably lower than that obtained with the PR-IM; the two only compounds detected were *o*-cresol and anisole, each one with a selectivity of approximately 50%. On the other hand, the conversion of methanol was approximately 20%, the products formed being dimethylether (with the co-product water) and 2,2-dimethoxypropane. The latter compound is the ketal formed by the acid-catalyzed reaction between acetone and methanol, the ketone likely being formed by dehydrogenation (via H-transfer) of isopropanol. The latter is the product of the acid-catalyzed hydration of propylene, the olefin typically being obtained by transformation of methanol over strongly acid sites. Therefore, the acidity offered by the IM-300 sample is strong enough to catalyze transformations of methanol. On the other hand, phenol cannot access the active sites, and does not react with methanol at all. This is also confirmed by IR spectra shown in Fig. 10, which showed that phenol interacts with few silanols and is adsorbed at the outer surface as phenolate species.

The spent IM-300 sample contained a minor amount of coke, which was much less than that accumulated on the PR-IM sample. Since the formation of coke is unlikely to occur inside the nanotubes of imogolite, this indicates that methanol reacted with both silanols inside the imogolite nanotubes, yielding lighter compounds (*i.e.* dimethylether and 2,2-dimethoxypropane), and also with the external Al(OH)Al sites, giving rise to the formation of heavier compounds and finally to coke.

Fig. 13 shows the behaviour of L-IM. This sample was much more active than IM-300; in fact, the conversion at 300 °C was low (≈3%), but nevertheless was two orders of magnitude higher than that of IM-300. Moreover, there are two relevant differences with respect to the performance of PR-IM (Figs. 11 and 12): (a) there was no evident deactivation phenomenon, which was

instead the case with PR-IM and (b) the distributions of products of the two materials were quite different. In fact, with L-IM the main product was *o*-cresol, showing a selectivity close to 80% regardless of temperature and conversion. At 450 °C, the selectivity to anisole was 10% and that to *p*-cresol was 4%, the only polyalkylated compound being 2,6-xylenol, formed with selectivity of 3%. With PR-IM, at the same temperature and for a similar value of phenol conversion, the selectivity to 2,6-xylenol was 8%, that to other polyalkylated phenols was 10% and that to *p*-cresol was 13%. This difference indicates that the type and strength of the active sites in the two materials were different.

*3.5.3. The reactivity of reference materials: alumina and silica*

In order to better understand the differences experimentally observed, we carried out reactivity tests with alumina (Fig. 14) and with silica (Fig. 15). Alumina was very active, showing 60% phenol conversion at 250 °C; a partial deactivation was responsible for the observed decrease of conversion at 390 °C. At low temperature, the prevailing product was anisole, the selectivity of which however decreased rapidly in favour of the formation of polyalkylated phenols, amongst which the prevailing one was 2,6-xylenol. This behaviour indicates the different activation energy between O-alkylation, leading to anisole, and C-alkylation, the latter being preferred at high temperature [45]. The prevalent mono-alkylated compound was *o*-cresol, *p*-cresol formed only in a trace amount. This behaviour also indicates the amphoteric behaviour of alumina in this reaction; the Al(OH)Al surface groups have an acidic behaviour towards methanol, which is activated with the formation of an electrophilic species. On the other hand, the surface has a basic behaviour to phenol, which adsorbs and generates a phenolate species, the protons being abstracted by the nucleophilic Al–O–Al oxygen [46–48]. Because of the repulsion between the aromatic ring and the surface, the phenolate adopts an orthogonal orientation; this adsorption mode favours the attack at the ortho position in phenol, and finally leads to the formation of *o*-cresol and 2,6-xylenol.

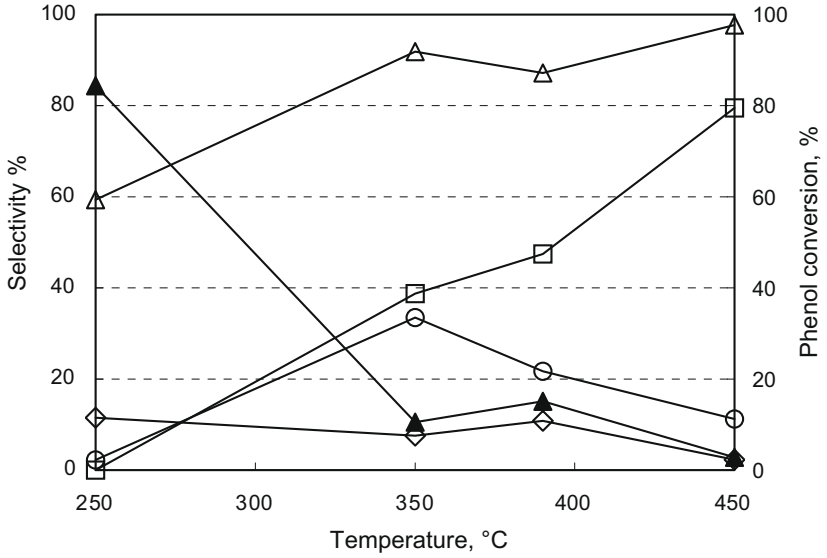


**Fig. 14.** Effect of temperature on catalytic performance of $Al_2O_3$. Symbols: phenol conversion (△), selectivity to *o*-cresol (◇), selectivity to anisole (▲), selectivity to 2,6-xylenol (○) and selectivity to other polyalkylated aromatics (□).

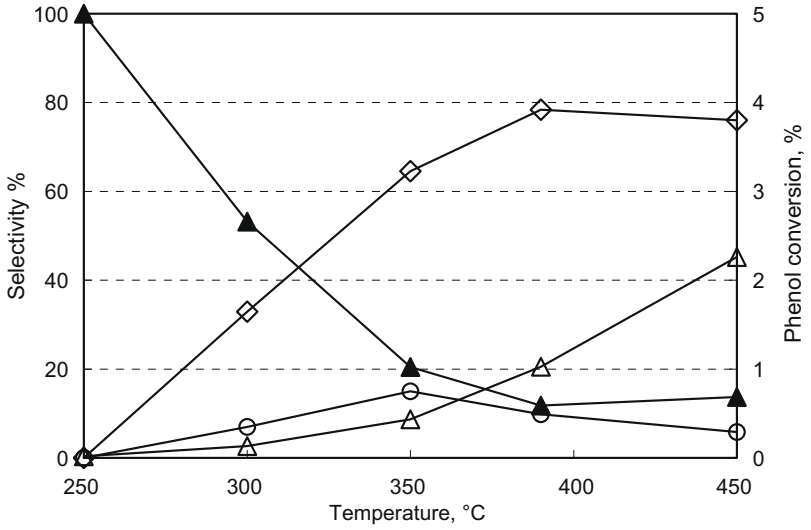


**Fig. 15.** Effect of temperature on catalytic performance of $SiO_2$. Symbols: phenol conversion (△), selectivity to *o*-cresol (◇), selectivity to anisole (▲), selectivity to 2,6-xylenol (○) and selectivity to other polyalkylated aromatics (□).

On silica, the conversion of phenol was very low because of the low acidity of surface silanols [23]; the low acidity is also the reason for the absence of any deactivation phenomenon. The only product at low temperature was anisole. The increase of temperature led to the preferred formation of *o*-cresol, with a negligible formation of *p*-cresol. Despite the very low conversion, the selectivity to 2,6-xylenol was higher than 10%.

Apart from the very different activity, the behaviour of the two reference materials was not much different; both yielded anisole in prevalence at low temperature, regardless of the conversion achieved, and both gave C-alkylation products at high temperature. The latter was either *o*-cresol, when the conversion achieved was low (*i.e.* on silica), or 2,6-xylenol and other polyalkylated aromatics, when the conversion was high (*i.e.* on alumina).

*3.5.4. Comparison of catalytic materials*

The distribution of products obtained in the gas-phase methylation of phenol over PR-IM is similar to that observed with reference compounds alumina and silica. The relevant deactivation phenomena confirm the existence of surface acidic sites having medium strength, as also evidenced by FT-IR characterization. One difference with respect to alumina and silica concerns the selectivity to *p*-cresol; the latter was 10–15% with PR-IM, whereas it was negligible with both reference compounds. The regio-selectivity in the ring-alkylation of phenol with methanol is regulated by the charge density of the O atom in the oxidic catalyst, the latter being lower with silico-aluminates and greater with ionic oxides typically showing a basic behaviour [49–53]. In general, highly nucleophilic O atoms not only generate the phenolate species, but also force the latter to adopt an orthogonal orientation with respect to the surface, finally leading to high regio-selective C-alkylation and to the preferred formation of *o*-cresol. Therefore, in total the PR-IM catalytic behaviour is more similar to that of a zeolite [39] than to that of alumina.

The behaviour of L-IM (Fig. 12) is different from those of both silica and alumina, and that of PR-IM. In fact, with L-IM the main product of reaction was *o*-cresol, at both low and high temperatures. Anisole formed with low selectivity at 300 °C; selectivity then increased when the reaction temperature was increased (10% at 450 °C), a behaviour opposite to that usually found with Brønsted acid-type materials.

In some aspects, the behaviour of L-IM is similar to that observed with basic materials [40], showing high chemo- (C-alkylation largely preferred over O-methylation) and regio- (ortho-C-alkylation largely preferred over para-C-alkylation) selectivity in the gas-phase phenol alkylation with methanol. This behaviour agrees with the experimental finding that L-IM gives the strongest interaction with phenol and generates phenolate species (Fig. 10). The high nucleophilicity of the O atom explains the regio-selectivity experimentally observed. On the other hand, the presence of medium-strength acidic sites is responsible for the small, but non-negligible formation of anisole. Therefore, L-IM appears to have amphoteric behaviour, resulting from the combined reactivity of the acidic and basic sites present on its surface. Strongly nucleophilic $O^{2-}$ ions are generated by the high-temperature dehydration of imogolite, leading to strained Al–O–Al(Si) bonds that easily open by abstraction of the acidic phenolic proton and coordination of the phenolate to the $Al^{3+}$ cation. The same occurs in strongly dehydrated alumina, where the nucleophilicity of the $O^{2-}$ is responsible for the "basic" behaviour of the solid towards phenol [46–48].

Another peculiarity of the L-IM material is the absence of relevant deactivation phenomena, as confirmed by the relatively low amount of coke accumulated on the catalyst. This behaviour is also typically observed with basic catalysts [39,40]; a contribution, however, deriving from the lamellar-type morphology of the sample, which may favour the counter-diffusion of products limiting the generation of the hydrocarbon-pool precursor of coke formation, cannot be excluded.

## 4. Conclusions

PR-IM has a markedly acidic character, leading to a catalytic behaviour very similar to that of zeolitic-type materials, as it concerns both the distribution of the reaction products and the presence of deactivation phenomena. Besides the overall lower surface area, the hollow spheres morphology of proto-imogolite allows methanol and phenol molecules to access active sites, both at the inner and outer surfaces of the particles.

With IM, several factors must be accounted for: first of all, below 300 °C, nanotubes are partially filled with water, and therefore, besides few inner silanols interacting with $NH_3$, only Al(OH)Al groups and few $Al^{3+}$ Lewis sites at the outer surface may be accessed by probes.

At 300 °C, water is definitely removed and the inner surface, covered by silanols, becomes actually accessible to bases with different strength, CO and $NH_3$, and to bigger molecules, *i.e.* methanol and phenol. Due to its bulky structure, however, phenol access to silanols is limited by geometric/diffusional constraints, leading to a non-negligible conversion of methanol, but to a quite negligible degree of phenol conversion. As to surface hydroxyls acidity, interaction with $NH_3$ is strong, probably due to multiple interactions of ammonia with more than one silanol since the inner surface is lined by SiOH groups, and to difficult diffusion across micrometre long nanotubes. However, the hypothesis that the unusual acidic behaviour of silanols may derive from a peculiar structural feature of the solid cannot be completely ruled out and deserves further studies.

Finally, L-IM develops both medium-strength acidic and basic surface features, which result into an "amphoteric" catalytic behaviour. FT-IR spectroscopy showed, on the one hand, the presence of acidic Brønsted-like sites, similar to hydroxyls in high Al-content alumina-silicates and mildly acidic zeolites: on the other hand, the presence of basic sites is shown by the formation of phenolate species upon phenol adsorption. Basic properties, indeed, lead to phenol de-protonation and to the preferred formation of *o*-cresol, with negligible formation of *p*-cresol, as usually observed with basic-type solids.

## Acknowledgments

The authors wish to thank INSTM Consortium (Istituto Nazionale di Scienza e Tecnologia dei Materiali) for financial support (PRISMA 2005 Project) and for PhD grant of SP; Prof. Piero Ugliengo (Dipartimento di Chimica IFM, Università degli Studi di Torino, Italy) for fruitful discussions and Dr. Sharon Ashbrook (University of St. Andrews, UK) for solid-state NMR measurements.

## References

[1] N. Yoshinaga, A. Aomine, Soil Sci. Plant Nutr. 8 (3) (1962) 22.
[2] P.D.G. Cradwick, V.C. Farmer, J.D. Russell, C.R. Masson, K. Wada, N. Yoshinaga, Nature Phys. Sci. 240 (1972) 187.
[3] V.C. Farmer, M.J. Adams, A.R. Fraser, F. Palmieri, Clay Miner. 18 (1983) 459.
[4] V.C. Farmer, A.R. Fraser, in: M.M. Mortland, V.C. Farmer (Eds.), Proceedings of the International Clay Conference, Elsevier, Amsterdam, 1978, p. 547.
[5] S.I. Wada, A. Eto, K. Wada, in: M.M. Mortland, V.C. Farmer (Eds.), Proceedings of the International Clay Conference, Elsevier, Amsterdam, 1978, p. 348.
[6] P.I. Pohl, J.-L. Faulon, D.M. Smith, Langmuir 12 (1996) 4463.
[7] S. Konduri, S. Mukherjee, S. Nair, Phys. Rev. B 74 (2006) 033401.
[8] R.K. Iller, The Chemistry of Silica: Solubility, Polymerization, Colloid and Surface Properties, and Biochemistry of Silica, John Wiley and Sons, New York, 1979.
[9] W.C. Ackerman, D.M. Smith, J.C. Huling, Y.-W. Kim, J.K. Bailey, C.J. Brinker, Langmuir 9 (1993) 1051.

[10] M.A. Wilson, G.s.H. Lee, R.C. Taylor, Clays Clay Miner. 50 (3) (2002) 348.
[11] L. Denaix, I. Lamy, J.Y. Bottero, Colloids Surf. A 158 (1999) 315.
[12] C.J. Clark, M.B. McBride, Clays Clay Miner. 32 (4) (1984) 291.
[13] R.L. Parfitt, A.D. Thomas, R.J. Atkinson, R.St.C. Smart, Clays Clay Miner. 22 (1974) 455.
[14] Y. Arai, M. McBeath, J.R. Bargar, J. Joye, J.A. Davis, Geochim. Cosmochim. Acta 70 (2006) 2492.
[15] J.B. Harsh, S.J. Traina, J. Boyle, Y. Tang, Clays Clay Miner. 40 (6) (1992) 700.
[16] S. Imamura, Y. Hayashi, K. Kajiwara, H. Hoshino, C. Kaito, Ind. Eng. Chem. Res. 32 (1993) 600.
[17] S. Imamura, T. Kokubu, T. Yamashita, Y. Okamoto, K. Kajiwara, H. Kanai, J. Catal. 160 (1996) 137.
[18] C. Morterra, G. Magnacca, Catal. Today 27 (1996) 497. and references therein.
[19] J.P. Gustafsson, Clays Clay Miner. 49 (1) (2001) 73.
[20] K.J. MacKenzie, M.E. Bowden, J.W.M. Brown, R.H. Meinhold, Clays Clay Miner. 37 (4) (1989) 317, and references therein.
[21] B.A. Goodman, J.D. Russell, B. Montez, E. Olfield, R.J. Kirkpatrick, Phys. Chem. Miner. 12 (1985) 342.
[22] J.J. Fitzgerald, C. Murali, C.O. Nebo, M.C. Fuerstenau, J. Colloid Interf. Sci. 151 (1991) 299.
[23] G. Ghiotti, E. Garrone, C. Morterra, F. Boccuzzi, J. Phys. Chem. 83 (1979) 2863.
[24] O. Cairon, T. Chevreau, J.-C. Lavalley, J. Chem. Soc. Faraday Trans. 94 (1998) 3039. and references therein.
[25] B. Bonelli, B. Onida, J.D. Chen, A. Galarneau, F. Di Renzo, F. Fajula, E. Garrone, Micropor. Mesopor. Mater. 67 (2004) 95.
[26] A. Givan, a. Loewenshuss, C.J. Nielsen, Vib. Spectrosc. 12 (1996) 1.
[27] P.Y. Storozhev, C.O. Areán, E. Garrone, P. Ugliengo, V.A. Ermoshin, A.A. Tsyganenko, Chem. Phys. Lett. 374 (2003) 439.
[28] I. Mirsojew, S. ernst, J. Weitkamp, H. Knözinger, Catal. Lett. 24 (1994) 235.
[29] E. Garrone, R. Chiappetta, G. Spoto, P. Ugliengo, A. Zecchina, F. Fajula, in: R. von Ballmoos, J.B. Higgins, M.M.j. Treacy (Eds.), Proceedings of the Ninth International Zeolite Conference, Montreal, 1992, Butterworth-Heinemann, 1993, p. 267.
[30] A. Zecchina, S. Bordiga, G. Spoto, D. Scarano, G. Petrini, G. leofanti, M. Padovan, C.O. Areán, J. Chem. Soc. Faraday Trans. 88 (1992) 2959.
[31] B. Onida, F. Geobaldo, F. Testa, F. Crea, E. Garrone, Micropor. Mesopor. Mater. 30 (1999) 119.
[32] B. Onida, L. Borello, B. Bonelli, F. Geobaldo, E. Garrone, J. Catal. 214 (2003) 191.
[33] W. Daniell, U. Schubert, R. Glöckler, A. Meyer, K. Noweck, H. Knözinger, Appl. Catal. A 196 (2000) 247.
[34] J.A. Lercher, C. Gründling, G. Eder-Mirth, Catal. Today 27 (1996) 353.
[35] A. Zecchina, L. Marchese, S. Bordiga, C. Pazè, E. Gianotti, J. Phys. Chem. B 101 (1997) 10128.
[36] T. Beutel, J. Chem. Soc. Faraday Trans. 94 (1998) 985.
[37] T. Mathew, M. Vijayaraj, S. Pai, B.B. Tope, S.G. Hegde, B.S. Rao, C.S. Gopinath, J. Catal. 227 (2004) 175.
[38] B. Morrow, A.J. McFarlan, J. Phys. Chem. 96 (1992) 1395.
[39] N. Ballarini, F. Cavani, L. Maselli, A. Montaletti, S. Passeri, D. Scagliarini, C. Flego, C. Perego, J. Catal. 251 (2007) 423.
[40] N. Ballarini, F. Cavani, L. Maselli, S. Passeri, S. Rovinetti, J. Catal. 256 (2008) 215.
[41] I.M. Dahl, S. Kolboe, J. Catal. 149 (1994) 458.
[42] M. Bregolato, V. Bolis, C. Busco, P. Ugliengo, S. Bordiga, F. Cavani, N. Ballarini, L. Maselli, S. Passeri, I. Rossetti, L. Forni, J. Catal. 245 (2007) 283.
[43] J.F. Haw, W. Song, D.M. Marcus, J.B. Nicholas, Acc. Chem. Res. 26 (2003) 317.
[44] Ø. Mikkelsen, S. Kolboe, Micropor. Mesopor. Mater. 29 (1999) 173.
[45] R.F. Parton, J.M. Jacobs, H. van Ooteghem, P.A. Jacobs, Stud. Surf. Sci. Catal. 46 (1989) 211.
[46] L.H. Klemm, J. Shabtai, D.R. Taylor, J. Org. Chem. 33 (1968) 1480.
[47] Y. Fu, T. Baba, Y. Ono, Appl. Catal. A 178 (1998) 219.
[48] S. Porchet, L. Kiwi-Minsker, R. Doepper, A. Renken, Chem. Eng. Sci. 51 (11) (1996) 2933.
[49] R.J. Davis, J. Catal. 216 (2003) 396.
[50] Y. Ono, J. Catal. 216 (2003) 406.
[51] G. Busca, Phys. Chem. Chem. Phys. 1 (1999) 723.
[52] A. Cimino, F.S. Stone, Adv. Catal. 47 (2002) 141.
[53] M. Barteau, Chem. Rev. 96 (1996) 1413.